ORIGINAL ARTICLE

Do all chlorophyll fluorescence emission wavelengths capture the spring recovery of photosynthesis in boreal evergreen foliage?

Chao Zhang[1,2,3] | Jon Atherton[1] | Josep Peñuelas[2,3] | Iolanda Filella[2,3] | Pasi Kolari[4] | Juho Aalto[4,5] | Hanna Ruhanen[6] | Jaana Bäck[7] | Albert Porcar-Castell[1]

[1] Optics of Photosynthesis Laboratory, Institute for Atmospheric and Earth System Research (INAR)/Forest Sciences, Viikki Plant Science Centre, University of Helsinki, Helsinki 00014, Finland

[2] CREAF, Center for Ecological Research and Forestry Applications, Bellaterra 08193, Spain

[3] CSIC, Global Ecology Unit CREAF-CSIC-UAB, Cerdanyola del Vallès 08193, Spain

[4] Department of Physics, University of Helsinki, Helsinki 00014, Finland

[5] Station for Measuring Forest Ecosystem–Atmosphere Relations II (SMEAR II), Hyytiälä Forestry Field Station, University of Helsinki, Korkeakoski 35500, Finland

[6] Natural Resources Institute Finland (Luke), Natural Resources and Bioproduction, Suonenjoki 77600, Finland

[7] Department of Forest Sciences, University of Helsinki, Helsinki 00014, Finland

Correspondence
C. Zhang and A. Porcar-Castell, Optics of Photosynthesis Laboratory, Institute for Atmospheric and Earth System Research (INAR)/Forest Sciences, Viikki Plant Science Centre, University of Helsinki, Helsinki, 00014, Finland.
Email: chao.x.zhang@helsinki.fi; joan.porcar@helsinki.fi

Abstract

Chlorophyll *a* fluorescence (ChlF) is closely related to photosynthesis and can be measured remotely using multiple spectral features as solar-induced fluorescence (SIF). In boreal regions, SIF shows particular promise as an indicator of photosynthesis, in part because of the limited variation of seasonal light absorption in these ecosystems. Seasonal spectral changes in ChlF could yield new information on processes such as sustained nonphotochemical quenching (NPQ_S) but also disrupt the relationship between SIF and photosynthesis. We followed ChlF and functional and biochemical properties of *Pinus sylvestris* needles during the photosynthetic spring recovery period to answer the following: (a) How ChlF spectra change over seasonal timescales? (b) How pigments, NPQ_S, and total photosynthetically active radiation (PAR) absorption drive changes of ChlF spectra? (c) Do all ChlF wavelengths track photosynthetic seasonality? We found seasonal ChlF variation in the red and far-red wavelengths, which was strongly correlated with NPQ_S, carotenoid content, and photosynthesis (enhanced in the red), but not with PAR absorption. Furthermore, a rapid decrease in red/far-red ChlF ratio occurred in response to a cold spell, potentially relating to the structural reorganization of the photosystems. We conclude that all current SIF retrieval features can track seasonal photosynthetic dynamics in boreal evergreens, but the full SIF spectra provides additional insight.

KEYWORDS

chlorophyll *a* fluorescence spectra, evergreen vegetation, F_{690}, F_{740}, fluorescence ratio, leaf PAR absorption, *Pinus sylvestris*, PSI fluorescence, sustained nonphotochemical quenching (NPQ_S)

1 | INTRODUCTION

Chlorophyll *a* fluorescence (ChlF) of leaves, thylakoids, and photo-systems has been extensively used to study the organization, func-tioning, and acclimation of the photosynthetic light-harvesting apparatus (Baker, 2008; Govindjee, 1995; Murchie & Lawson, 2013; Porcar-Castell et al., 2014). ChlF can now be measured within discrete wavelengths from plant canopies, forest stands, and whole ecosystems with instrumentation on towers, drones, aircraft, and satellites (Joiner, Yoshida, Guanter, & Middleton, 2016; Parazoo et al., 2018; Porcar-Castell et al., 2015; Rascher et al., 2015; Sun et al., 2017; Zarco-Tejada, Catalina, González, & Martín, 2013). Widely addressed as solar-induced fluorescence (SIF) by the remote sensing community, SIF opens up the study of photosynthesis at unprecedented scales (Frankenberg et al., 2011, 2014; Parazoo et al., 2014; Sun et al., 2018; Thum et al., 2017; Zhang, Guanter, Joiner, Song, & Guan, 2018; Zuromski et al., 2018). This capacity could not only serve to improve the current accuracy of global car-bon budgets (Damm et al., 2015; Quéré et al., 2018; Smith et al., 2018) but also yield new understanding on the responses and feed-backs between terrestrial ecosystems and the environment, both critical milestones for the implementation of climate change mitigation and adaptation strategies (IPCC-SR15, 2018; Smith et al., 2014).

Despite the mounting evidence of the strong link between SIF and gross primary productivity (GPP) accumulating from ground, airborne, and satellite platforms (Guanter et al., 2014; Magney et al., 2019; Migliavacca et al., 2017; Parazoo et al., 2018; Sun et al., 2017; Zarco-Tejada, González-Dugo, & Fereres, 2016; Zuromski et al., 2018), the physical and biological mechanisms that underpin the rela-tionship and the potential wavelength-dependent information content in the SIF signal remain unclear (Porcar-Castell et al., 2014; Verrelst et al., 2016; Wieneke et al., 2018; Yang et al., 2018). This lack of understanding is particularly acute for evergreen foliage, where the seasonal link between SIF and GPP involves processes other than changes in absorbed photosynthetically active radiation (PAR), which could decouple and add wavelength dependencies to the relationship between SIF and GPP.

In contrast to pulse–amplitude–modulation (PAM) ChlF measure-ments, which integrate ChlF over a broad range of wavelengths, SIF is retrieved within narrow and discrete spectral bands around the red and far-red ChlF emission peaks (atmospheric oxygen absorption bands or solar Fraunhofer lines; Alonso et al., 2007; Meroni et al., 2009). Accordingly, because the shape of the leaf-level ChlF spectra is driven by a combination of physical, physiological, and biochemical factors (Magney et al., 2019), it can be expected that the seasonal rela-tionship between SIF and GPP would depend on retrieval wavelength, especially in boreal evergreen vegetation undergoing remarkable adjustments during the season.

A light use efficiency type model (Monteith, 1972) becomes a con-venient theoretical framework to introduce the physical and biological factors that couple (or decouple) SIF and GPP and connect the leaf-level phenomenology to the spatial scale of remote sensing. The inten-sity of the SIF signal emitted from a leaf or a plant canopy at a given wavelength (λ) can be expressed as a function of four factors: (a) the incoming PAR, (b) the fraction of that PAR absorbed by the leaf or can-opy (A), (c) the quantum yield of fluorescence with its associated emis-sion wavelength ($\Phi_F(\lambda)$), and (d) a wavelength-dependent escape probability ($f_{esc}(\lambda)$) that accounts for the reabsorption of predomi-nantly red ChlF photons by chlorophyll (Chl) molecules within the antenna, thylakoid, chloroplast, leaf, or plant canopy (Buschmann, 2007; Porcar-Castell et al., 2014; Romero, Cordon, & Lagorio, 2018; Yang & van der Tol, 2018) as follows:

$$SIF(\lambda) = PAR \cdot A \cdot \Phi_F(\lambda) \cdot f_{esc}(\lambda). \quad (1)$$

In similar terms, leaf or canopy level GPP can be expressed as follows:

$$GPP = PAR \cdot A \cdot LUE, \quad (2)$$

where LUE corresponds to the photosynthetic light use efficiency in moles of CO_2 assimilated moles per mole of absorbed PAR photons. By combining equations (note that A and PAR cancel out), a simple the-oretical relationship that links GPP to SIF can be obtained as follows:

$$GPP = \frac{1}{f_{esc}(\lambda)} \cdot \frac{LUE}{\Phi_F(\lambda)} \cdot SIF(\lambda). \quad (3)$$

In this equation, widely applied to the interpretation of remotely sensed SIF data (Damm et al., 2015; Frankenberg & Berry, 2018; Guanter et al., 2014; Lee et al., 2015; van der Tol, Berry, Campbell, & Rascher, 2014), physical factors (e.g., structure-dependent ChlF reabsorption) are embedded in the $1/f_{esc}(\lambda)$ term, and biological fac-tors (e.g., architecture and physiological state of the light reactions, alternative energy sinks, cyclic electron transport, and photorespira-tion) are embedded in the $LUE/\Phi_F(\lambda)$ term. Clearly, any seasonal changes in the strength of the factors above can potentially couple and decouple SIF and GPP (Porcar-Castell et al., 2014). In addition, any seasonal changes in the leaf-level wavelength properties of $f_{esc}(\lambda)$ and $\Phi_F(\lambda)$ can add wavelength dependencies to the link between SIF(λ) and GPP, something that remains to be characterized.

Seasonal changes in leaf Chl content, although usually modest in boreal evergreens (Ensminger et al., 2004; Öquist & Huner, 2003; Porcar-Castell, Juurola, et al., 2008), affect light absorption and also $f_{esc}(\lambda)$ via ChlF reabsorption (Buschmann, 2007). Similarly, structural changes at the level of chloroplast and thylakoid membrane, for exam-ple, thylakoid grana unstacking and aggregation of Chl binding light-harvesting complexes in overwintering evergreens (Demmig-Adams, Muller, Stewart, Cohu, & Adams, 2015; Öquist, Chow, & Anderson,

1992; Ruban, 2016; Ruban, Johnson, & Duffy, 2012; Verhoeven, 2014), could also contribute to the modulation of $f_{esc}(\lambda)$ potentially affecting the spectral properties of SIF and its seasonal correlation to GPP.

$\Phi_F(\lambda)$ is composed of at least two components: a highly dynamic component that responds to photochemical quenching (PQ) and nonphotochemical quenching (NPQ) of excitation energy in photosystem II (PSII) and that fluoresces in the red and far-red regions (Franck, Juneau, & Popovic, 2002; Palombi et al., 2011) and a component from photosystem I (PSI) assumed to remain stationary over the short term (Genty, Wonders, & Baker, 1990; Palombi et al., 2011; Pfündel, Klughammer, Meister, & Cerovic, 2013) that fluoresces predominantly in the near infrared. Accordingly, if seasonal dynamics in sustained NPQ (NPQ$_S$; Öquist & Huner, 2003; Ottander, Campbell, & Öquist, 1995; Verhoeven, 2014) quenched only the ChlF components from PSII, one would expect NPQ$_S$ to affect the spectral properties of $\Phi_F(\lambda)$. Similarly, differences in the patterns of seasonal photoinhibition of PSII (Ensminger et al., 2004; Murata, Takahashi, Nishiyama, & Allakhverdiev, 2007) and PSI reaction centres (Huang, Yang, Hu, & Zhang, 2016; Sonoike, 2011) could also affect the ChlF spectra and its spectral dependency with photosynthesis.

In summary, although a strong seasonal coupling between PAM ChlF and photosynthesis has been widely reported for evergreen foliage (e.g., Ensminger et al., 2004; Kolari et al., 2014; Ottander & Öquist, 1991; Soukupová et al., 2008; Springer, Wang, & Gamon, 2017; Zarter, Demmig-Adams, Ebbert, Adamska, & Adams, 2006), the spectral dependency of the relationship remains unresolved.

The objective of the study was to characterize the seasonal variation of ChlF spectra for boreal evergreen Scots pine needles during the spring recovery of photosynthesis. Hence, we investigated if red and far-red wavelengths of ChlF were equally positioned to capture the spring recovery of photosynthesis. To do so, we combined long-term and continuous *in situ* measurements of gas exchange and PAM ChlF with repeated measurements of foliar pigment content, leaf total PAR absorption, and spectral ChlF, spanning the full dynamic range of variation in photosynthetic capacity of Scots pine needles: from deeply downregulated foliage during winter to fully functional foliage during peak growing season in summer.

2 | MATERIALS AND METHODS

2.1 | Study site and field sampling protocol

Measurements were conducted at Hyytiälä/SMEAR-II (Station for Measuring Forest Ecosystem-Atmosphere Relations) in Southern Finland (61°51′N, 24°17′E, 181 m a.s.l.; Hari & Kulmala, 2005), in a 52-year-old Scots pine (*Pinus sylvestris* L.) stand with a dominant height of approximately 18 m. The study period (February 24 to July 20, 2015) encompassed three biological seasons: end of winter (full dormant state), spring, and first half of summer (peak growing season).

The study combined continuous *in situ* measurements of micrometeorological variables, CO_2 exchange, and PAM ChlF across four different trees (N = 4), with repeated point measurements of steady-

state spectral ChlF at room temperature and pigment analysis across five trees (previous four plus one, N = 5). Spectral ChlF was purposefully measured under standardized PAR so that it could serve as a proxy of $\Phi_F(\lambda)$ in Equations (1) and (3) (i.e., absorbed PAR assumed constant). To avoid changing the needle cohort in the middle of the experiment, all measurements were conducted in the newest cohort of needles available at the start of the study period (developed in summer 2014). To avoid defoliation effects, several branches from the four topmost whorls were selected per tree and used for the repeated sampling of needles. Needles were sampled always before 10 a.m. Overall, the study included a total of 19 measuring points in addition to the continuous measurements (Figure 1).

2.2 | Continuous measurements of micrometeorological data and shoot CO_2 exchange

Air temperature (°C; Pt100 sensor) and PAR (μmol m^{-2} s^{-1}; Li-190SZ, Li-Cor Inc., Lincoln, NE, USA) were measured right above the forest at 1 min intervals from sensors placed in a tall mast. The CO_2 exchange of pine shoots was measured in top canopy shoots 30–60 times per day using a system of automated dynamic chambers coupled to an infrared gas analyser (Li-840, Li-Cor Inc., Lincoln, NE, USA; see, e.g., Aalto et al., 2014, for further details). Chambers remained open most of the time exposing the studied shoots to ambient conditions and closed only during measurement. Fluxes were estimated from the change in CO_2 concentration during the first 40 s upon chamber closure (Kolari et al., 2012). Shoots with fully developed needles from 2014 were debudded prior to chamber installation to prevent new growth during the study period and for practical reasons. Total needle area inside the chamber was measured at the end of the study period and used to calculate fluxes. A total of two to four chambers (N = 2–4) were used during the study period from February 24 to July 20 in 2015 (Figure S1a).

Direct comparison of noon LUE from chamber data (moles CO_2 assimilated/moles PAR absorbed) can be problematic in boreal conditions due to low PAR levels during the winter months. Accordingly, we decided to use here a simple model of photosynthesis (the optimal stomatal control model; Hari, Mäkelä, Korpilahti, & Holmberg, 1986; Kolari, Lappalainen, Hänninen, & Hari, 2007) that allows robust estimation of photosynthetic parameters under ambient CO_2 concentrations, low light, and low temperatures (Kolari et al., 2014). Two key photosynthetic parameters were estimated in a 3-day time window to capture the seasonal development in LUE: (a) α (μmol CO_2/μmol PAR), the slope of a linear function fitted to the photosynthetic light response with low incident PAR (<300 μmol m^{-2} s^{-1}) before noon (Figure S1b; Kolari et al., 2014). Under constant leaf PAR absorption (Figure S2), this parameter can be considered a measure of maximum photosynthetic LUE under low light. In addition, and because our spectral ChlF measurements were not conducted under low light, we also estimated (b) β (m s^{-1}), the maximum rate of light-saturated photosynthesis per unit intercellular CO_2 concentration (Figure S1c). This parameter can be considered a measure of light-saturated
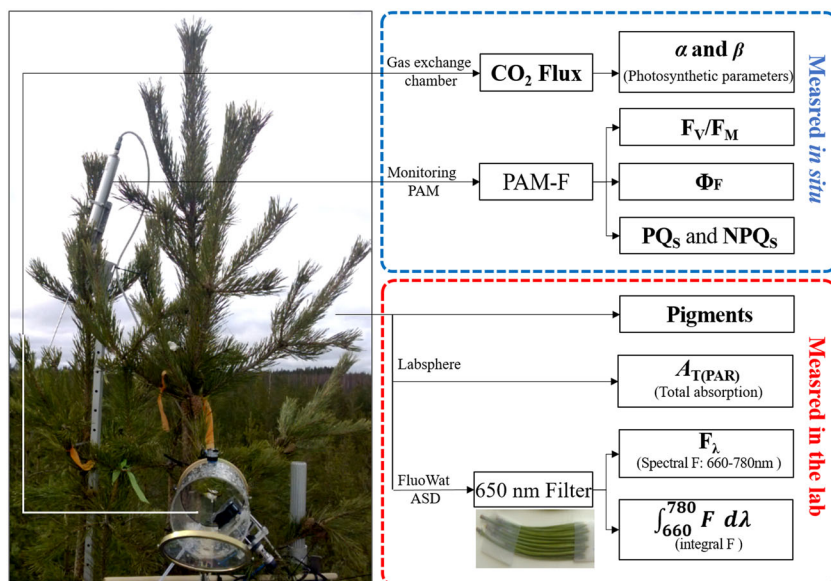
FIGURE 1 Measurement rationale during the spring recovery of 2015 in *Pinus sylvestris*. *In situ* measurements encompassed (a) continuous gas exchange measurements with automated chambers (N = 2–4 trees) to estimate CO_2 flux and derive the seasonal photosynthetic parameters α and β, and (b) continuous PAM fluorescence measurements (N = 4) to derive maximum quantum yield of PSII (F_V/F_M), quantum yield of fluorescence (Φ_F), and sustained photochemical (PQ_S) and nonphotochemical quenching (NPQ_S).For the lab measurement, needles from top branches (N = 5) were sampled during each measuring day. One portion was immediately frozen in liquid nitrogen for posterior pigments analysis. Another portion was rapidly brought to the laboratory, and used to measure total PAR absorption ($A_{T(PAR)}$) and spectral fluorescence (F_λ) respectively (see also Materials and methods section for details) [Colour figure can be viewed at wileyonlinelibrary.com]

photosynthesis at optimal temperature, low vapour pressure deficit, and ambient CO_2 concentration.

We normalized α and β parameters to their mean values between May 3 and 23 (see Figure S1d,e). This is a common procedure in time-series analysis and serves to minimize the impact of systematic variability and emphasize the seasonal patterns in the data, which was our goal. The normalization period was selected in May as that was the time when all four chambers were simultaneously recording and the foliage was already photosynthetically active. Normalized unit-less values were then converted back to the original units by multiplying the normalized values by the respective means across all four chambers. The parameters α and β are used hereinafter as a measure of the seasonal spring recovery of photosynthesis.

2.3 | Continuous measurements of PAM ChlF *in situ*

A Monitoring PAM system (MONI-PAM, Walz GmbH, and Germany; Porcar-Castell, 2011; Porcar-Castell, Pfündel, Korhonen, & Juurola, 2008), equipped with four independent PAM fluorometers, was used to record the instantaneous fluorescence yield (F'), the maximal fluorescence yield (F'_M), incoming PAR, and temperature every 30 min. Night F' and F'_M were assumed to correspond to minimal (F_o) and maximal (F_M) fluorescence and used to derive daily maximum quantum yield of PSII, F_V/F_M after Kitajima and Butler (1975), and to calculate quenching parameters NPQ_S and PQ_S after Porcar-Castell (2011) as follows: $NPQ_S = F_{MR}/F_M - 1$ and $PQ_S = F_{MR}/F_o - F_{MR}/F_M$, where F_{MR} is the summer night reference obtained for those particular needles in the absence of NPQ_S. A decrease in PQ_S relative to summer levels was here interpreted in terms of photoinhibition of reaction centres (Porcar-Castell, 2011). Finally, seasonal changes in PAM based fluorescence yield (Φ_F) were estimated as $\Phi_F = 0.1\ F_o/F_{MR}$ (Porcar-Castell, 2011, note the unfortunate typo in

equation 24 therein where F'_M should be F_{MR}), which is based on the assumption of a maximum fluorescence yield of 10% for PSII particles at the F_M state (Barber, Malkin, & Telfer, 1989). The four fluorometers were installed in top canopy branches pointing south.

2.4 | Validation of ChlF measurements

For practical reasons, this study compared ChlF spectra of cut needles measured under standard conditions and at room temperature, with photosynthetic parameters (α, β, F_V/F_M, NPQ_S, and PQ_S,) obtained from the field instrumentation. Accordingly, we wanted to test that our measurements at room temperature correctly represented the same physiological state as measurements carried out in the field. In addition, we wanted to ensure that our MONI-PAM system (which consistently supplied 48 light pulses per day to the same needles throughout the study period) was not introducing any long-term artefact. We used a Hansatech fluorometer (FMS-2, Hansatech Instruments Ltd., Kings Lynn, Norfolk, UK) to measure F_V/F_M both in the field and under standardized conditions indoors. During each sampling point, we placed a total of 25 dark-acclimation clips, distributed across the five study trees, and dark acclimated for at least 1 hr prior to measuring F_V/F_M. The same measurements were subsequently repeated at room temperature using collected needles instead. As expected, F_V/F_M obtained from the FMS-2 in the field was highly correlated with estimates from the MONI-PAM system (r = 0.97, P < 0.0001; Figure S3), denoting that the MONI-PAM system did not introduce any bias into the observed seasonal patterns. The small discrepancy between slopes is very likely due to differences in the colour of the measuring light as well as the ChlF detection range between instruments. Similarly, F_V/F_M measurements obtained with the FMS-2 fluorometer in field were found to be strongly correlated with those of detached needles at room temperature (r = 0.94, P < 0.0001; Figure S3),

suggesting that room temperature measurements did not introduce any major bias into the observed seasonal patterns in spectral ChlF.

2.5 | Estimation of foliar pigment content

During each sampling point, five pairs of needles per tree were randomly detached using the preselected top branches and needle cohort. Needles were sampled into cryotubes, immediately frozen at liquid nitrogen temperature using a portable dewar (CX-100, Taylor Wharton International LLC, Minnetonka, MN), and subsequently stored at −80 °C until extraction. Pigment analysis were conducted following Wellburn (1994) with dimethyl sulfoxide (VWR Chemicals, 23500.322) as solvent. Frozen samples (75–100 mg) were first homogenized for 2 min at 30 Hz, using a bead mill (TissueLyser II Qiagen, Germany), stainless steel beads (4 mm), and microtubules (2 ml). Subsequently, 1.8 ml of dimethyl sulfoxide was added to the homogenate and resuspended again at 30 Hz for 1 min. Pigments were extracted in oven at 40 °C for 4 hr. Extracts were then centrifuged at 25,000 g for 5 min. Light absorption was measured at 649.1, 665.1, and 480.0 nm, with a spectrophotometer (Shimadzu UV-2401 PC), and subsequently used for estimation of Chl a, Chl b, and total carotenoids (Wellburn, 1994).

2.6 | Measurements of leaf absorption

Needle PAR absorption ($A_{T(PAR)}$) was measured eight times during the study period ($N = 5$ biological replicates). We used the same spectrometer and LED light source described above connected to a 6-inch diameter integrating sphere (AdaptaSphere, LabSphere Inc., New Hampshire, UK) and applied the black spray method (Olascoaga, Mac, Atherton, & Porcar-Castell, 2016) to estimate $A_{T(PAR)}$. The black spray method was inspired by earlier within-sphere measurements (Idle & Proctor, 1983; Öquist, Hällgren, & Brunes, 1978) and purposefully developed to measure absorption in leaves with complex geometry, like needles, because it does not require mounting needles in the port of the integrating sphere, and therefore, there are no gap effects. Instead, samples are placed inside the sphere and hung from a white thread across the central plane (see illustrations in Olascoaga et al.,2016 for details). Prior to measurements, five to six needle pairs were separated and the resulting 10–12 needles sewed with a white thread and spaced at least 1 cm. The method consisted of three separate spectral measurements inside the sphere: (1) white thread alone (reference zero absorption, I_W), (2) white thread with needles (sample absorption, I_S), and (3) white thread with needles painted with a black spray of known absorption (black sample, I_B). Conveniently, because the total surface area of the needles in steps 2 and 3 can be assumed to remain constant, this parameter cancels out and there is no need to estimate it. Total PAR absorption can then be computed by combining these three measurements with the known absorption of the black spray (A_{BLACK}) as follows:

$$A_T = \frac{(I_W - I_S)\, I_B\, A_{BLACK}}{(I_W - I_B)\, I_S}. \tag{4}$$

The mean value of A_T between 400 and 700 nm was here used as an estimate of $A_{T(PAR)}$.

2.7 | Room temperature measurements of leaf spectral ChlF

Leaf spectral ChlF (F_λ, in mW m^{-2} sr^{-1} nm^{-1}) was measured at room temperature using a FluoWat Clip (Image Processing Laboratory, University of Valencia, Spain; Van Wittenberghe, Alonso, Verrelst, Moreno, & Samson, 2015) coupled with a powerful white LED (MJ-858, Magicshine, UK) and a radiometrically calibrated visible-near-infrared spectrometer (FieldSpec, ASD-Panalytical, Boulder, CO). The spectrometer covers the spectral range between 325 and 1075 nm at a sampling interval of 1 nm and with a FWHM of 3.5 nm. The FluoWat clip has an optical window for input illumination (incidence angle of 45°) and a small aperture (at nadir view) to connect the optical fibre. The fibre field of view is 25°, and the distance to sample is 1 cm, yielding an approximately circular target area of 0.22-cm radius. To obtain spectral ChlF, a 650-nm short-pass filter (Edmund Optics Ltd., UK; OD = 4) was used to exclude 99.99% of radiation above 650 nm. The LED source supplies a PAR of approximately 1,200 μmol at the leaf surface as estimated with a PAR sensor (Licor LI150-A, Li-Cor Inc., Lincoln, NE, USA).

Needles were carefully arranged alongside each other to minimize the gap fraction and fixed with transparent tape to conform a needle mat (see Figure 1). Rajewicz, Atherton, Alonso, and Porcar-Castell (2019) recently compared the ChlF spectra of needles with different arrangements and concluded that despite the fact that needle mats could slightly enhance reabsorption, they provided a higher replicability and reproducibility and were therefore a good solution to track temporal changes in spectral properties.

Needle mats were dark adapted at 10 °C for 1 hr and kept in the dark until measurements started in the FluoWat clip. After conducting a dark current measurement, the needle mat was placed in the FluoWat clip, recording was started, and an opaque aluminium foil placed between the light source and the FluoWat clip rapidly removed. Variations of spectral ChlF were recorded during 2 min at an integration time of 136 ms. The last 10 spectra were averaged and used to estimate steady-state ChlF between 650 and 850 nm (F_λ). Averaged spectra were further smoothed using a Savitzky–Golay filter (order = 2, averaging interval = 15) and cut to a range of 660–780 nm where the signal was strongest. The resulting fluorescence spectra were used to estimate red (F_{690}) and far-red ChlF (F_{740}) and used to calculate an integrated steady-state ChlF between 660 and 780 nm ($\int_{660}^{780} F d\lambda$) for correspondence with the broadband PAM fluorescence parameter, Φ_F.

2.8 | Statistical analyses

Mean values of four (gas exchange and Monitoring PAM fluorescence) or five (all other data) trees were used to conduct statistical analysis. Linear regression models and simple Pearson's correlation analyses were used to assess relationships between variables. All the analyses were conducted with R version 3.2.2 (R Core Development Team, 2015) and MATLAB version R2014a (MathWorks Inc., 2014).

Principal component analysis (PCA) was used to quantitatively assess the relative role of different components of variation in the spectral ChlF dataset. In particular, we wanted to quantify how much of the seasonal variation in spectral ChlF during the spring recovery of photosynthesis was related to principal components associated with changes in the intensity and how much was related to principal components associated with changes in the shape. The R function "prcomp" in the default mode (prcomp arguments; scale = FALSE and centre = TRUE) was used to run a PCA on time series of the ChlF dataset. The analysis was focused on the 660 to 780 nm emission region to reduce impact of low signal-to-noise at wavelength limits.

3 | RESULTS

3.1 | Seasonal changes in micrometeorological variables and photosynthetic parameters

Both temperature and PAR followed the typical annual pattern in boreal regions with PAR increasing faster and earlier than temperature (Figure 2a). Daily mean temperatures in February (−1.7 °C) and March (0.6 °C) were higher by 6 °C and 4 °C, respectively, compared with the average for the period 1981–2010 (Pirinen et al., 2012). Fortunately, a cold spell took place on March 22 with a daily mean temperature of −5.7 °C. On April 16, a second cold spell took place with a mean temperature of 0.7 °C. These cold spells served to assess the responses of ChlF and photosynthetic parameters to a sudden decrease in temperature and were highlighted in figures reporting the time series.

Noon mean CO_2 fluxes (Figure 2b) registered a clear seasonal pattern gradually increasing from April to June. Both α (a measure of maximum LUE under low light) and β (a measure of maximum photosynthetic rate) displayed similar seasonal patterns (Figure 2c), gradually increasing from winter to summer. The effect of the cold spells on α and β parameters could not be distinguished.
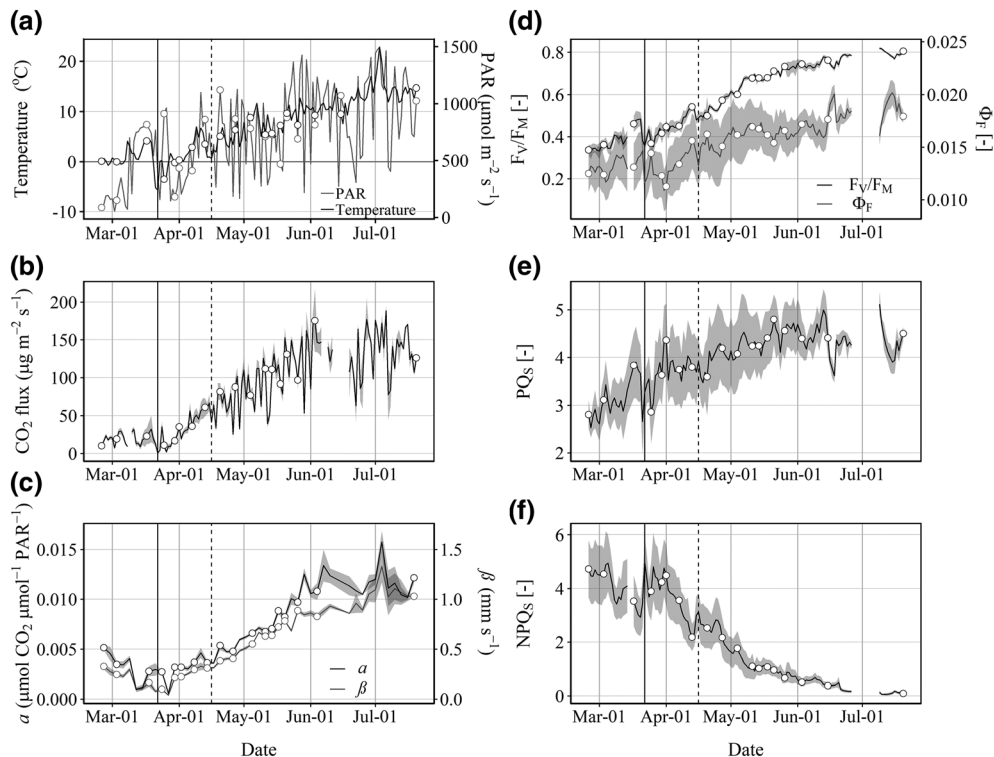
FIGURE 2 Seasonal variation of meteorological and photosynthetic parameters. (a) Daily mean temperature (°C; *black line*) and mean midday photosynthetically active radiation between 11:00 and 14:00 (PAR; μmol m^{-2} s^{-1}; *grey line*), (b) mean midday CO_2 flux between 11:00 and 14:00 (μg m^{-2} s^{-1}), (c) proxies of maximum photosynthetic light-use efficiency (α; *black line*) and maximum photosynthetic rate (β; *grey line*) in prevailing conditions estimated from the gas exchange data, (d) daily maximum quantum yield of PSII (F_V/F_M; *black line*) and quantum yield of fluorescence(Φ_F; *grey line*), and (e) sustained photochemical (PQ$_S$) and (f) nonphotochemical (NPQ$_S$) quenching measured using MONI-PAM. Lines indicate the continuous measurement. Open points represent the dates when sampling took place. Solid and vertical black line indicates the first cold spell on March 22, and dotted and vertical black line indicates the second cold spell on April 16. Points in b-f represent means of four biological replicates (N = 4). Shadows represent ±SE

Changes in the F_V/F_M and Φ_F (Figure 2d) measured in the field with the MONI-PAM system also tracked the development of the spring recovery of photosynthesis, rapidly decreasing in response to the two cold spells and gradually recovering from winter to summer. Over the full spring recovery, Φ_F varied approximately by a factor of 2 from its minimum in early April to its maximum in June and July. Variations in F_V/F_M were further decomposed into PQ_S and NPQ_S components (Figure 2e,f). NPQ_S presented larger seasonal variation decreasing from about 5 at the beginning of the study period to zero during summer. In contrast, PQ_S increased from values of about 3 at the beginning of the study period to values of 4.5 during summer. Both NPQ_S and PQ_S consistently responded to both cold spells, increasing and decreasing, respectively.

3.2 | Seasonal changes in pigment content and leaf absorption

No obvious seasonal patterns were observed in total Chl levels (Figure 3a) although a slightly decreasing trend occurred during spring, which reversed towards summer. This result was consistent with the time series of total leaf PAR absorption ($A_{T(PAR)}$, Figure S2), which did not display any seasonal pattern either with values ranging from 0.81 to 0.85. In contrast, seasonal changes were observed in Chl b (Figure 3c), Chl a/b (Figure 3d), carotenoid content (Figure 3e), and Car/Chl ratios (Figure 3f). During early spring, Chl a/b ratios were lower and carotenoid and Car/Chl ratios higher than during summer. No clear effects of the cold spells were seen in the pigments, except for Chl a/b, which displayed higher levels after the second cold spell, and Car/Chl, which had a tendency to increase after the cold spells.

3.3 | Seasonal variation in ChlF spectra

The ChlF spectra of pine needles measured at room temperature and at standard illumination (F_λ, Figure 4a–c) was used here as a proxy of variations in the spectrally resolved fluorescence yield. F_λ experienced strong seasonal changes during the study period, mainly in terms of intensity but also in shape. For example, the red peak near 690 nm was nearly absent during winter (Figure 4a,b) but gradually reappeared towards summer (Figure 4c). Both red (F_{690}) and far-red (F_{740}) ChlF (Figure 4d) increased from early spring to summer with a larger change in F_{740}. Integrated ChlF ($\int_{660}^{780} Fd\lambda$; Figure 4e), used here for comparison with the spectrally averaged Φ_F, presented a similar seasonal pattern with the rest of photosynthetic parameters. Both Φ_F (Figure 2d) and $\int_{660}^{780} Fd\lambda$ (Figure 4e) varied seasonally by a factor of 2. The F_{690}/F_{740} ratio drastically decreased from 0.5 to 0.4 in response to the first cold spell and did not reverse to 0.5 until several weeks later (Figure 4f). Later on, the ratio decreased again to about 0.45 by the end of the study period, coinciding with the increase in total Chl (Figure 3a) and F_λ (Figure 4d).
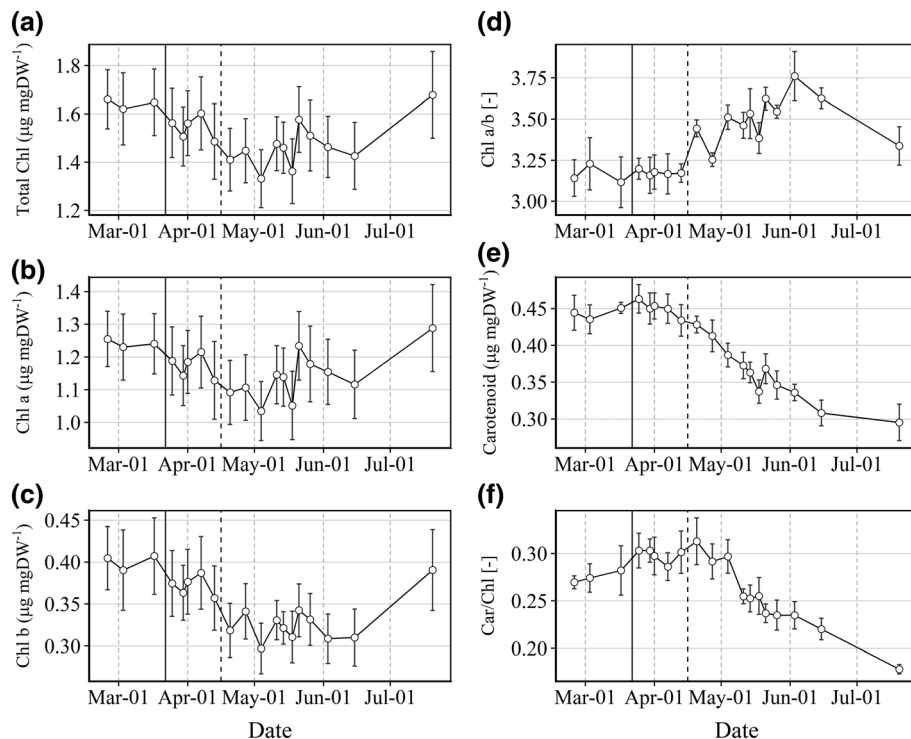
FIGURE 3 Seasonal variation of foliar pigment content. (a) Total chlorophyll (Chl; $\mu g\,mgDW^{-1}$), (b) Chlorophyll a (Chl a; $\mu gmgDW^{-1}$), (c) Chlorophyll b (Chl b; $\mu g\,mgDW^{-1}$), (d) Chlorophyll a / Chlorophyll b (Chl a/b), (e) Total carotenoid ($\mu g\,mgDW^{-1}$), and (f) Carotenoid/Chlorophyll ratio (Car/Chl). Solid and vertical black line indicates the first cold spell on March 22, and the dotted and vertical black line indicates the second cold spell on April 16. Points represent means of five biological replicates(N = 5). Error bars represent ±SE
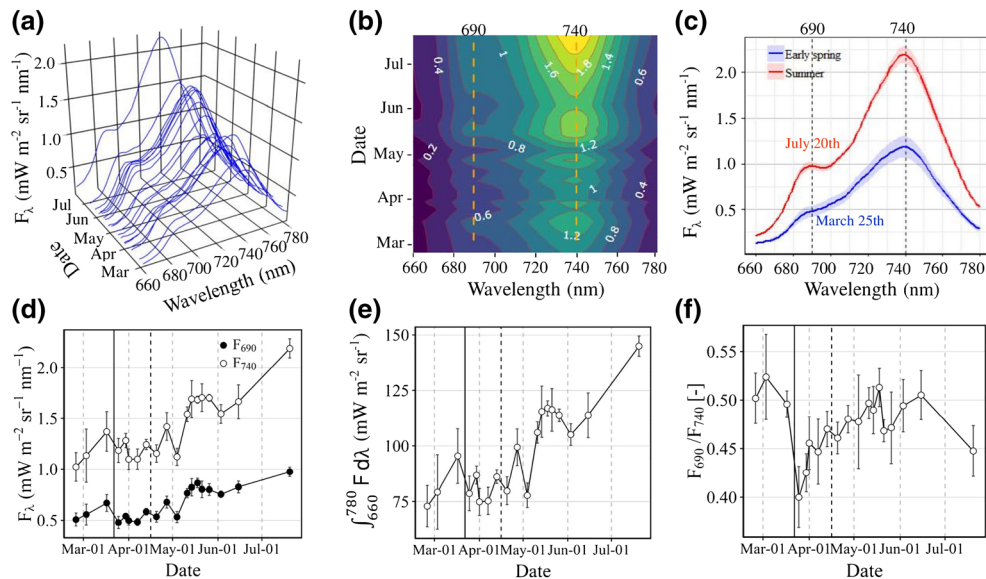
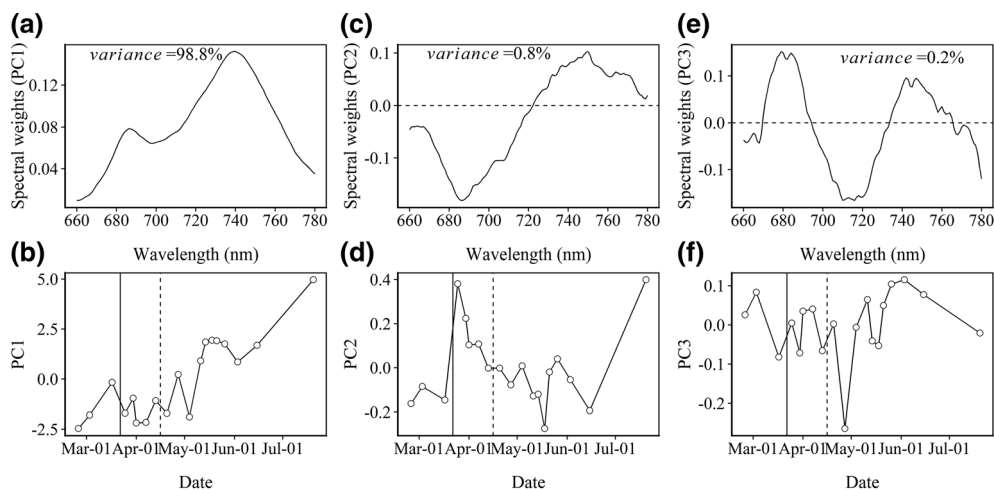**FIGURE 4** Seasonal variation in spectral chlorophyll fluorescence (ChlF). (a-c) The shape of spectral ChlF from 680 to 770 nm (F_λ; mW m^{-2} sr^{-1} nm^{-1}). The contour figure of (b) indicate the F_λ values. Two examples of spectral ChlF in (c) were measured on March 25 (early spring), and July 20 (summer), (d) Red ChlF at 690 (F_{690}; *filled circles*) and far-red ChlF at 740 nm (F_{740}, *open circles*), (e) integral ChlF from 660 to 780 nm, and (f) fluorescence ratio (F_{690}/F_{740}). Solid and vertical black line indicates the first cold spell on March 22, and the dotted and vertical black line indicates the second cold spell on April 16. Shadows in c and error bars ind-f represent ±SE (N = 5)

3.4 | Principal component analysis

Three principal components explained 99.8% of the variation in ChlF spectra during the study period (Figure 5). PC1 explained 98.8% of variance of ChlF spectra across the spring recovery (Figure 5a) and exhibited a clear and similar seasonal pattern (Figure 5b) to that of red, far-red, and integrated ChlF (Figure 4d,e). The spectral weights and intensity of PC1 reflected the shape and seasonal variation in Φ_F. In contrast, PC2 (Figure 5c) explained only 0.8% of variance but its spectral weights presented a strong and wavelength-dependent shape reflecting

differences in red and far-red ChlF. PC2 potentially indicates seasonal changes in ChlF reabsorption (i.e., $f_{esc}(\lambda)$ in Equation 1), changes in energy redistribution between PSII and PSI, or changes in the emission spectra at the photosystem level. Remarkably, a drastic increase of PC2 (Figure 5d) was detected upon the first cold spell (solid and vertical black line), and later on during summer when foliar Chl content tended to increase (Figure 3a). Overall, the seasonal pattern of PC2 closely resembled the mirror image of F_{690}/F_{740} (Figure 4f). PC3 explained only 0.2% of variance (Figure 5e) and displayed no clear seasonal trend other than a sharp decrease at the end of April (Figure 5f).

FIGURE 5 Principal component analysis (PCA) for spectral chlorophyll fluorescence. Panels indicate spectral variability (*top panels*) and seasonal patterns (*bottom panels*) of PC1 (a,b), PC2 (c,d) and PC3 (e,f) respectively. Solid and vertical black line indicates the first cold spell on March 22, and dotted and vertical black line indicates the second cold spell on April 16

	α	β	CO_2 flux	F_V/F_M	Φ_F	PQ_S	NPQ_S	Total Chl	Chl a/b	Carotenoid	Car/Chl	$A_{T(PAR)}$	F_{690}	F_{740}	$\int_{660}^{780} F\, d\lambda$	F_{690}/F_{740}	PC1	PC2	PC3
α	1	0.98	0.85	0.89	0.79	0.66	-0.87	-0.16	0.76	-0.97	-0.87	0.04	0.83	0.81	0.81	0.31	0.81	-0.02	0.29
β	0.98	1	0.87	0.94	0.8	0.75	-0.91	-0.19	0.77	-0.98	-0.86	0.07	0.86	0.84	0.84	0.33	0.84	-0.06	0.26
CO_2 flux	0.85	0.87	1	0.93	0.84	0.78	-0.92	-0.37	0.88	-0.86	-0.66	-0.29	0.76	0.72	0.73	0.35	0.73	-0.15	0.16
F_V/F_M	0.89	0.94	0.93	1	0.87	0.87	-0.98	-0.36	0.8	-0.94	-0.78	0.04	0.89	0.87	0.87	0.34	0.87	-0.14	0.16
Φ_F	0.79	0.8	0.84	0.87	1	0.56	-0.94	-0.48	0.76	-0.84	-0.6	0.25	0.73	0.71	0.72	0.28	0.72	-0.1	0.12
PQ_S	0.66	0.75	0.78	0.87	0.56	1	-0.78	-0.33	0.63	-0.73	-0.57	-0.13	0.74	0.71	0.72	0.28	0.72	-0.16	0.05
NPQ_S	-0.87	-0.91	-0.92	-0.98	-0.94	-0.78	1	0.43	-0.81	0.92	0.72	-0.05	-0.86	-0.83	-0.84	-0.35	-0.83	0.16	-0.12
Total Chl	-0.16	-0.19	-0.37	-0.36	-0.48	-0.33	0.43	1	-0.51	0.3	-0.2	0.22	-0.11	-0.01	-0.03	-0.28	-0.03	0.37	0.14
Chl a/b	0.76	0.77	0.88	0.8	0.76	0.63	-0.81	-0.51	1	-0.77	-0.55	-0.4	0.59	0.52	0.53	0.37	0.53	-0.27	0.45
Carotenoid	-0.97	-0.98	-0.86	-0.94	-0.84	-0.73	0.92	0.3	-0.77	1	0.87	-0.15	-0.9	-0.87	-0.87	-0.41	-0.87	0.17	-0.25
Car/Chl	-0.87	-0.86	-0.66	-0.78	-0.6	-0.57	0.72	-0.2	-0.55	0.87	1	-0.18	-0.87	-0.87	-0.87	-0.3	-0.87	0.03	-0.36
$A_{T(PAR)}$	0.04	0.07	-0.29	0.04	0.25	-0.13	-0.05	0.22	-0.4	-0.15	-0.18	1	0.18	0.3	0.29	-0.64	0.3	0.51	-0.34
F_{690}	0.83	0.86	0.76	0.89	0.73	0.74	-0.86	-0.11	0.59	-0.9	-0.87	0.18	1	0.97	0.98	0.42	0.98	-0.2	0.04
F_{740}	0.81	0.84	0.72	0.87	0.71	0.71	-0.83	-0.01	0.52	-0.87	-0.87	0.3	0.97	1	1	0.19	1	0.05	0.02
$\int_{660}^{780} F\, d\lambda$	0.81	0.84	0.73	0.87	0.72	0.72	-0.84	-0.03	0.53	-0.87	-0.87	0.29	0.98	1	1	0.25	1	-0.02	0
F_{690}/F_{740}	0.31	0.33	0.35	0.34	0.28	0.28	-0.35	-0.28	0.37	-0.41	-0.3	-0.64	0.42	0.19	0.25	1	0.23	-0.92	0.08
PC1	0.81	0.84	0.73	0.87	0.72	0.72	-0.83	-0.03	0.53	-0.87	-0.87	0.3	0.98	1	1	0.23	1	0	0
PC2	-0.02	-0.06	-0.15	-0.14	-0.1	-0.16	0.16	0.37	-0.27	0.17	0.03	0.51	-0.2	0.05	-0.02	-0.92	0	1	0
PC3	0.29	0.26	0.16	0.16	0.12	0.05	-0.12	0.14	0.45	-0.25	-0.36	-0.34	0.04	0.02	0	0.08	0	0	1

FIGURE 6 Pearson correlation (r) matrix between key study variables. The r value is indicated as colour (positive correlations are shaded blue, and negative correlations are shaded orange) and number [Colour figure can be viewed at wileyonlinelibrary.com]

3.5 | Seasonal correlations between photosynthetic parameters and spectral ChlF

Measurements of red, far-red, and integral ChlF under standardized conditions were strongly correlated with field photosynthetic parameters α (r: 0.81–0.83), β (r: 0.84–0.86), and F_V/F_M (r: 0.87–0.89; $P < 0.001$ for all; Figures 6 and S4). In contrast, no significant relationships between F_{690}/F_{740} and photosynthetic parameters were found. Red (F_{690}) and far-red (F_{740}) ChlF were strongly and negatively correlated also with leaf carotenoid content (r: −0.9 and −0.87, respectively) and NPQ_S (r: −0.86 and −0.83, respectively) and positively related with Φ_F (r: 0.73 and 0.71, respectively) and PQ_S (r: 0.74 and 0.71, respectively; $P < 0.001$ for all; Figures 6 and S4). In fact, NPQ_S and leaf carotenoid content were the two factors that displayed the strongest (negative) correlation with the spring recovery of photosynthesis in terms of α, β, and F_V/F_M. No significant relationship was observed between red or far-red ChlF and total Chl or $A_{T(PAR)}$ (Figure S4).

As for the principal components, PC1 was correlated strongly with F_V/F_M ($r = 0.87$); negatively correlated with carotenoid, Car/Chl, and NPQ_S (r: −0.87 to −0.83); and had a significant but slightly lower relationship with Φ_F and PQ_S ($r = 0.72$; $P < 0.001$ for all; Figures 6 and S4). PC2 was highly and negatively correlated with F_{690}/F_{740} ($r = −0.92$; $P < 0.001$) but was not significantly correlated with $A_{T(PAR)}$ ($r = 0.51$) and total Chl ($r = 0.37$). Finally, PC3 was only marginally correlated with Chl a/b ($r = 0.45$; $P = 0.06$).

We also conducted a systematic assessment of the seasonal correlations between different ChlF emission wavelengths and photosynthetic parameters (Figure 7). The results indicated that both red and far-red ChlF wavelengths were strongly correlated with the spring recovery of photosynthesis ($P < 0.001$ for all), represented here by the photosynthetic parameters α and β (Figure 7a), with red wavelengths displaying stronger correlations than far-red wavelengths. Correlations were also stronger for β, compared with α across the whole spectral range, which is not surprising because our spectral measurements were conducted at high light. The strength of the correlation decreased between the two ChlF emission peak, with highest RMSE (data not shown). As expected, a wavelength dependency in the slope of α (β) versus F_λ was also observed (Figure 7b), further emphasizing that the ratio LUE/$\Phi_F(\lambda)$ (as in Equation 3) was dependent on ChlF emission wavelengths. Positive intercepts of F_λ versus α (β) (Figure 7c; with ranges of 0.15 to 0.95 mW m^{-2} sr^{-1} nm^{-1}) were obtained for both parameters and across wavelengths, indicating positive ChlF emission when photosynthetic gas exchange approaches zero.

Additionally, all the main ChlF emission wavelengths from 680 to 770 nm were well correlated with Φ_F ($P < 0.001$ for all) and presented slightly stronger relationships in the red region than far-red (Figure S5a). This was consistent with better correlations of ChlF with photosynthetic parameters in the red than in the far-red wavelengths (Figure 7a). Further, when comparing F_λ with $\int_{660}^{780} F d\lambda$, red wavelengths presented slightly lower correlations (Figure S5b), reflecting that red ChlF fluorescence wavelengths account for a source of independent information not conveyed by broadband ChlF.

4 | DISCUSSION

We followed the spectral response of ChlF during the spring recovery of photosynthesis. We found an across wavelength increase in ChlF "level" well correlated with photosynthetic parameters and additional subtler changes in spectral shape over time. Critically, photosystems
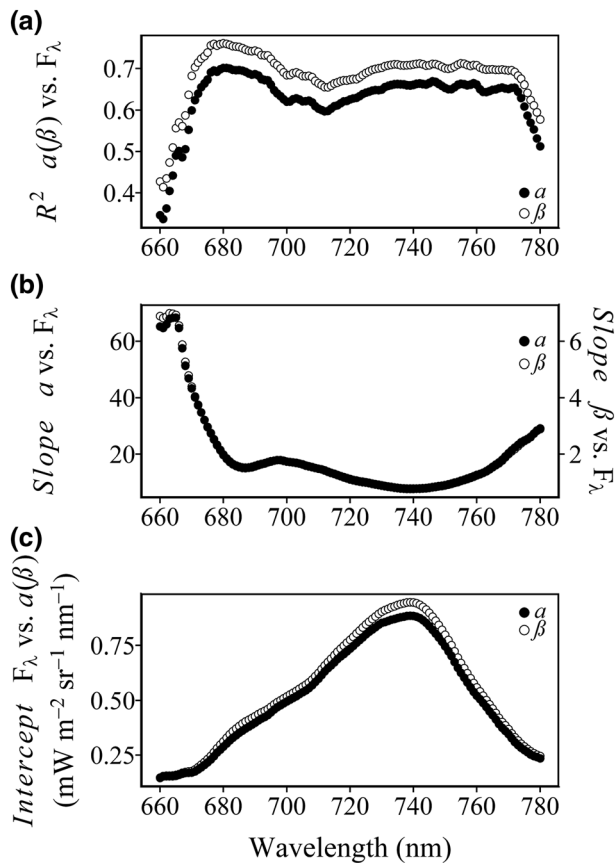
FIGURE 7 The linear regression between individual spectral fluorescence from 660 to 780 nm (F_λ) and photosynthetic parameters (α, filled circles and β, open circles). (a) Coefficients of determination (R^2), (b) slopes of α (β) vs. F_λ, and (c) intercepts of F_λ vs. α (β)

in overwintering evergreens undergo major structural and biochemical adjustments during the nonphotosynthetic season (Adams & Demmig-Adams, 1994; Ensminger et al., 2004; Gilmore & Ball, 2000; Ottander et al., 1995; Verhoeven, 2014), which were reflected in the variation of the measured ChlF spectra.

4.1 | Seasonal variation in leaf-level ChlF spectra and its controls

We used PCA analysis to separate and quantify the relative roles of different components of variation in the seasonal ChlF dynamics of pine needles. We found that 98.8% of the seasonal variation in ChlF spectra of needles was explained by changes in ChlF level (PC1) with only a marginal 1% of variation associated with additional changes in shape (with PC2 explaining 0.8%). Factors contributing to these components of variation are discussed next.

Lack of correlation between F_{690}, F_{740} (and PC1), and total Chl content or $A_{T(PAR)}$ (Figures 6 and S4) evidenced the minor role of PAR absorption in driving the seasonality of ChlF during the spring recovery. In the present study, Chl content remained relatively stable (Figure 3a). This is at odds with previous work where significant

seasonal changes in Chl content have been observed in Scots pine needles (Ensminger et al., 2004; Ottander et al., 1995; Porcar-Castell et al., 2012) and other evergreen species (Wong & Gamon, 2015). It is unclear why we observed such differences in pigments, but considering the alternative scenario where Chl did change during the season, and as the bulk of the spring recovery of ChlF in Scots pine needles has been shown to precede the summer increase in foliar Chl content by about 2 weeks (Porcar-Castell, et al., 2008), changes in leaf PAR absorption (A, Equation 1) will likely remain of lesser importance in controlling the seasonality in leaf-level SIF(λ) in evergreen conifers. We also did not find evidence of an inverse and persistent relationship between red/far-red ratio and foliar Chl content across the study period (Figures 6 and S4), as would follow from the general Chl reabsorption theory (Figure 4a in Gitelson, Buschmann, & Lichtenthaler, 1999, and Figure 4 in Buschmann, 2007). This result demonstrates that, in addition to foliar Chl content, other factors also influence the shape of the ChlF spectra.

Seasonal changes in both F_{690} and F_{740} (and PC1) were strongly related to seasonal variation in foliar carotenoid content, NPQ_S, and, to a lesser extent, PQ_S (Figure 6). The mechanisms that drive NPQ_S in overwintering evergreens (understood as the sustained enhancement in the capacity for thermal dissipation of excitation energy) remain under intense investigation (Demmig-Adams & Adams, 2006; Malnoë, 2018; Ruban, 2016; Verhoeven, 2014). NPQ_S in evergreens has been associated to the accumulation of carotenoids (especially zeaxanthin) relative to Chl (Adams & Demmig-Adams, 1994; Ensminger et al., 2004; Porcar-Castell et al., 2012; Zarter et al., 2006), the accumulation of damaged or nonfunctional PSII reaction centers coupled to a reduction in the PSII core D1 protein (Ebbert, Adams, Mattoo, Sokolenko, & Demmig-Adams, 2005; Ensminger et al., 2004; Ottander et al., 1995), the presence and accumulation of early light-induced proteins with or without concomitant changes in minor antenna PsbS proteins (Ebbert et al., 2005; Ensminger et al., 2004; Verhoeven, 2014; Zarter, Demmig-Adams, et al., 2006), the aggregation of light-harvesting complexes of PSII (LHCII; Busch, Hüner, & Ensminger, 2007; Horton et al., 1991; Ottander et al., 1995; Ruban, 2018), and the unstacking of the thylakoid membrane (Demmig-Adams et al., 2015).

Reversible forms of NPQ, which operate in time scales of seconds to minutes, (e.g., energy-dependent or zeaxanthin-dependent quenching qE and qZ, respectively; Malnoë, 2018; Verhoeven, 2014), are known to predominantly quench ChlF associated with PSII units with no apparent effect on PSI ChlF (Franck et al., 2002; Genty et al., 1990). As a result, because the ChlF contribution from PSI is much larger around the far-red peak (Franck et al., 2002; Genty et al., 1990; Pfündel, 1998), an increase in qE or qZ results in a reduction in the red/far-red ChlF ratio (Agati, Cerovic, & Moya, 2000; Agati, Mazzinghi, Fusi, & Ambrosini, 1995). If the PSI ChlF contribution would be also insensitive to NPQ_S, we would have expected a similar decrease in F_{690}/F_{740} in response to the seasonal accumulation of NPQ_S. This scenario was not fully supported by our observations because the extremes of variation in F_{690}/F_{740} ratio (observed during March; Figure 4f) took place under comparable Chl and NPQ_S levels

(Figures 2f and 3a), suggesting that PSI ChlF contribution is dynamic at the seasonal scale.

Seasonal changes in the ChlF ratio are clearly driven by multiple controls. For example, F_{690}/F_{740} decreased from 0.5 to 0.4 in response to the first cold spell, along with an increase in NPQ_S (Figure 2f) and in PC2 (Figure 5d), which occurred under rather stable Chl content (Figure 3a). This phenomena could denote a structural reorganization at the level of LHCII (increased reabsorption due to aggregation) or thylakoid membrane unstacking (promoting energetic connectivity between PSII and PSI units) accompanying the accumulation of NPQ_S. In fact, similar decreases in red/far-red ChlF ratio have been reported in response to reversible NPQ-induced oligomerization of LHCII complexes (Jahns & Holzwarth, 2012; Miloslavina et al., 2008). Later on, in mid-May and July, we registered a slight increase in foliar Chl content (Figure 3a) accompanied by a decrease in the F_{690}/F_{740} ratio (Figure 4f) and under rather stable NPQ_S (Figure 2f) corresponding to the previous characterized relationship between leaf Chl content and the ChlF ratio (Gitelson et al., 1999). Overall, further experimental and modelling studies are needed to clarify the mechanisms that drive the dynamics in the ChlF spectra in overwintering evergreens.

4.2 | Wavelength dependency between ChlF and photosynthesis

We found that all the main ChlF emission wavelengths (680–770 nm) were correlated with and capable of tracking the photosynthetic spring recovery in boreal evergreen foliage (Figure 7a). This finding was consistent with the dominant role of NPQ_S in controlling the seasonal variability in the ChlF level across wavelengths (PC1; Figure 5a,b). It is important to note, however, that the relative contributions of the variation in spectral shape (1% for PC2 + PC3) and ChlF level (98.8% for PC1) to total seasonal variation in ChlF spectral properties could have been very different in a different species or under a different set of environmental conditions, encouraging further seasonal studies across other species and biomes.

Slightly higher correlations (Figure 7a) and slopes (Figure 7b) were found between red wavelengths of F_λ and α and β. Similar results have been reported at the canopy scale based on model simulations (Liu et al., 2019; Verrelst et al., 2015) and experimental data (Campbell et al., 2019; Cheng et al., 2013; Magney, Bowling, et al., 2019). At the leaf level, the higher correlation in red wavelengths could point to interferences with the dynamics or PSI ChlF in the far-red wavelengths. In fact, the spectral shape of the intercept (Figure 7c), which represents the background ChlF spectra at zero photosynthesis, had a high resemblance to the typical spectral shape of PSI ChlF, although the peak was slightly red shifted (740 nm) compared with earlier studies in non-downregulated leaves of barley (722 nm; Franck et al., 2002) or maize PSI particles (725–730 nm; Croce, Dorra, Holzwarth, & Jennings, 2000). Further work to characterize and identify the drivers of this background ChlF signal, which may have important

implications for interpretation of SIF data over boreal evergreen regions, is needed.

4.3 | Implications at the larger scale

SIF is a promising methodology for the estimation of GPP dynamics in terrestrial ecosystems either using statistical methods based on Equation (3) (Guanter et al., 2014; Li et al., 2018; Sun et al., 2017) or by assimilation into the photosynthetic modules of land surface models (Lee et al., 2015; Macbean et al., 2018; Thum et al., 2017). SIF could be particularly useful for evergreen ecosystems by capturing part of the temporal dynamics of GPP that remains hidden to traditional reflectance-based vegetation indices due to low variation in greenness (Magney, Bowling, et al., 2019; Nichol et al., 2019; Smith et al., 2018; Walther et al., 2016; Zuromski et al., 2018).

Overall, our results indicate that current Fraunhofer- and oxygen-based methods to retrieve SIF across different wavelengths in the red and near-infrared regions (Lu, Cheng, Li, & Tang, 2018; Meroni et al., 2009) have similar intrinsic potential to capture the leaf-level spring recovery of photosynthesis in boreal evergreen forests. Importantly, when upscaling from the leaf to the canopy and landscape level, the constancy assumption behind the $LUE/\Phi_F(\lambda)$ factor in Equation (3) will be further complicated by spatial variation in physiological factors caused by within canopy light and temperature gradients or species composition (Porcar-Castell et al., 2014; Sun et al., 2017). Similarly, canopy-level f_{esc} (Equation 3) will be also affected by seasonal dynamics in canopy structure related to the phenology of the multiple components in the ecosystem, including the understory (Liu et al., 2019; Majasalmi, Stenberg, & Rautiainen, 2017).

5 | CONCLUSIONS

We demonstrated that red and far-red ChlF emission wavelengths were able to transmit the optical signature of the spring recovery of photosynthesis in boreal evergreen needles. The dynamics of the spectral signature were mediated by the complex and highly articulated process of sustained regulatory thermal dissipation or NPQ_S, which effectively quenches all ChlF wavelengths. Although changes in the shape of the ChlF spectra explained only a marginal proportion of the observed seasonality, the information content embedded in these changes could be highly informative. Specifically, the rapid decrease in the F_{690}/F_{740} ratio upon the first cold spell suggests that in addition to Chl content, F_{690}/F_{740} can also convey information on the structural organization in the thylakoid membrane in overwintering evergreens, which could help to better constrain the assimilation of SIF data into models of photosynthesis (Macbean et al., 2018; Raczka et al., 2019). Further investigations across species and scales will be required to fully characterize the information potentially embedded in the spectral dynamics of SIF, in support of multispectral SIF retrievals from towers, drones, airplanes, and satellite missions such as current TROPOspheric Monitoring Instrument, TROPOMI, onboard Sentinel-5 (Guanter et al.,

2015; Köhler et al., 2018) or future Fluorescence Explorer mission, FLEX (Drusch et al., 2017).

CONFLICT OF INTEREST

The authors have no conflicts of interest to declare.

AUTHOR CONTRIBUTIONS

Albert Porcar-Castell, Jon Atherton, Iolanda Filella, Josep Peñuelas, and Jaana Bäck conceived and designed the study; Chao Zhang and Albert Porcar-Castell carried out the optical measurements; Chao Zhang and Jon Atherton conducted the majority of the data analysis; Pasi Kolari estimated the photosynthetic parameters; Juho Aalto carried out and processed the field gas exchange data at SMEAR-II station; Hanna Ruhanen conducted the pigments analysis; Chao Zhang and Albert Porcar-Castell wrote the paper with contributions from all authors.

ORCID

Chao Zhang https://orcid.org/0000-0001-7327-9477
Josep Peñuelas https://orcid.org/0000-0002-7215-0150
Iolanda Filella https://orcid.org/0000-0001-6262-5733
Pasi Kolari https://orcid.org/0000-0001-7271-633X
Jaana Bäck https://orcid.org/0000-0002-6107-667X
Albert Porcar-Castell https://orcid.org/0000-0003-1357-9982

REFERENCES

Aalto, J., Kolari, P., Hari, P., Kerminen, V. M., Schiestl-Aalto, P., Aaltonen, H., … Bäck, J. (2014). New foliage growth is a significant, unaccounted source for volatiles in boreal evergreen forests. *Biogeosciences*, *11*, 1331–1344. https://doi.org/10.5194/bg-11-1331-2014

Adams, W. W., & Demmig-Adams, B. (1994). Carotenoid composition and down regulation of photosystem II in three conifer species during the winter. *Physiologia Plantarum*, *92*, 451–458. https://doi.org/10.1111/j.1399-3054.1994.tb08835.x

Agati, G., Cerovic, Z. G., & Moya, I. (2000). The effect of decreasing temperature up to chilling values on the in vivo F685/F735 chlorophyll fluorescence ratio in *Phaseolus vulgaris* and *Pisum sativum*: The role of the photosystem I contribution to the 735 nm fluorescence band. *Photochemistry and Photobiology*, *72*, 75–84. https://doi.org/10.1562/0031-8655(2000)072<0075:TEODTU>2.0.CO;2

Agati, G., Mazzinghi, P., Fusi, F., & Ambrosini, I. (1995). The F685/F730 chlorophyll fluorescence ratio as a tool in plant physiology: Response to physiological and environmental factors. *Journal of Plant Physiology*, *145*, 228–238. https://doi.org/10.1016/S0176-1617(11)81882-1

Alonso L., Gómez-chova L., Vila-francés J., Amorós-lópez J., Guanter L., Calpe J. & Moreno J. (2007) Sensitivity analysis of the Fraunhofer Line Discrimination method for the measurement of chlorophyll fluorescence using a field spectroradiometer. IEEE, 3756–3759.

Baker, N. R. (2008). Chlorophyll fluorescence: A probe of photosynthesis in vivo. *Annual Review of Plant Biology*, *59*, 89–113. https://doi.org/10.1146/annurev.arplant.59.032607.092759

Barber, J., Malkin, S., & Telfer, A. (1989). The origin of chlorophyll fluorescence in vivo and its quenching by the photosystem II reaction centre. *Philosophical Transactions of the Royal Society B: Biological Sciences*, *323*, 227–239. https://doi.org/10.1098/rstb.1989.0006

Busch, F., Hüner, N. P. A., & Ensminger, I. (2007). Increased air temperature during simulated autumn conditions does not increase photosynthetic carbon gain but affects the dissipation of excess energy in seedlings of the evergreen conifer jack pine. *Plant Physiology*, *143*, 1242–1251. https://doi.org/10.1104/pp.106.092312

Buschmann, C. (2007). Variability and application of the chlorophyll fluorescence emission ratio red/far-red of leaves. *Photosynthesis Research*, *92*, 261–271. https://doi.org/10.1007/s11120-007-9187-8

Campbell, P. K., Huemmrich, K. F., Middleton, E. M., Ward, L. A., Julitta, T., Daughtry, C. S., … Kustas, W. P. (2019). Diurnal and seasonal variations in chlorophyll fluorescence associated with photosynthesis at leaf and canopy scales. *Remote Sensing*, *11*, 1–36.

Cheng, Y., Middleton, E. M., Zhang, Q., Huemmrich, K. F., Campbell, P. K. E., Corp, L. A., … Daughtry, C. S. (2013). Integrating solar induced fluorescence and the photochemical reflectance index for estimating gross primary production in a cornfield. *Remote Sensing*, *5*, 6857–6879. https://doi.org/10.3390/rs5126857

Croce, R., Dorra, D., Holzwarth, A. R., & Jennings, R. C. (2000). Fluorescence decay and spectral evolution in intact photosystem I of higher plants. *Biochemistry*, *39*, 6341–6348. https://doi.org/10.1021/bi992659r

Damm, A., Guanter, L., Paul-limoges, E., Tol, C., Der, V., Hueni, A., … Schaepman, M. E. (2015). Far-red sun-induced chlorophyll fluorescence shows ecosystem-specific relationships to gross primary production: An assessment based on observational and modeling approaches. *Remote Sensing of Environment*, *166*, 91–105. https://doi.org/10.1016/j.rse.2015.06.004

Demmig-Adams, B., & Adams, W. W. (2006). Photoprotection in an ecological context: The remarkable complexity of thermal energy dissipation. *New Phytologist*, *172*, 11–21. https://doi.org/10.1111/j.1469-8137.2006.01835.x

Demmig-Adams, B., Muller, O., Stewart, J. J., Cohu, C. M., & Adams, W. W. (2015). Chloroplast thylakoid structure in evergreen leaves employing strong thermal energy dissipation. *Journal of Photochemistry and Photobiology B: Biology*, *152*, 357–366. https://doi.org/10.1016/j.jphotobiol.2015.03.014

Drusch, M., Moreno, J., Del Bello, U., Franco, R., Goulas, Y., Huth, A., … Verhoef, W. (2017). The FLuorescence EXplorer Mission Concept-ESA's Earth Explorer 8. *IEEE Transactions on Geoscience and Remote Sensing*, *55*, 1273–1284. https://doi.org/10.1109/TGRS.2016.2621820

Ebbert, V., Adams, W. W., Mattoo, A. K., Sokolenko, A., & Demmig-Adams, B. (2005). Up-regulation of a photosystem II core protein phosphatase inhibitor and sustained D1 phosphorylation in zeaxanthin-retaining, photoinhibited needles of overwintering Douglas fir. *Plant, Cell and Environment*, *28*, 232–240. https://doi.org/10.1111/j.1365-3040.2004.01267.x

Ensminger, I., Sveshnikov, D., Campbell, D. A., Funk, C., Jansson, S., Lloyd, J., … Öquist, G. (2004). Intermittent low temperatures constrain spring recovery of photosynthesis in boreal Scots pine forests. *Global Change Biology*, *10*, 995–1008. https://doi.org/10.1111/j.1365-2486.2004.00781.x

Franck, F., Juneau, P., & Popovic, R. (2002). Resolution of the Photosystem I and Photosystem II contributions to chlorophyll fluorescence of intact leaves at room temperature. *Biochimica et Biophysica Acta - Bioenergetics*, *1556*, 239–246. https://doi.org/10.1016/S0005-2728(02)00366-3

Frankenberg, C., & Berry, J. (2018). Solar induced chlorophyll fluorescence: Origins, relation to photosynthesis and retrieval. In *Reference module in earth systems and environmental sciences: Comprehensive remote sensing* (pp. 143–162). Oxford: Elsevier.

Frankenberg, C., Fisher, J. B., Worden, J., Badgley, G., Saatchi, S. S., Lee, J. E., … Yokota, T. (2011). New global observations of the terrestrial carbon cycle from GOSAT: Patterns of plant fluorescence with gross primary productivity. *Geophysical Research Letters*, *38*, 1–6.

Frankenberg, C., O'Dell, C., Berry, J., Guanter, L., Joiner, J., Köhler, P., … Taylor, T. E. (2014). Prospects for chlorophyll fluorescence remote sensing from the Orbiting Carbon Observatory-2. *Remote Sensing of Environment*, *147*, 1–12. https://doi.org/10.1016/j.rse.2014.02.007

Genty, B., Wonders, J., & Baker, N. R. (1990). Non-photochemical quenching of F_o in leaves is emission wavelength dependent: Consequences for quenching analysis and its interpretation. *Photosynthesis Research*, *26*, 133–139. https://doi.org/10.1007/BF00047085

Gilmore, A. M., & Ball, M. C. (2000). Protection and storage of chlorophyll in overwintering evergreens. *Proceedings of the National Academy of Sciences*, *97*, 11098–11101. https://doi.org/10.1073/pnas.150237697

Gitelson, A. A., Buschmann, C., & Lichtenthaler, H. K. (1999). The chlorophyll fluorescence ratio F_{735}/F_{700} as an accurate measure of the chlorophyll content in plants. *Remote Sensing of Environment*, *69*, 296–302. https://doi.org/10.1016/S0034-4257(99)00023-1

Govindjee, G. (1995). Sixty-three years since Kautsky: Chlorophyll *a* fluorescence. *Australian Journal of Plant Physiology*, *22*, 131–160.

Guanter, L., Aben, I., Tol, P., Krijger, J. M., Hollstein, A., Köhler, P., … Landgraf, J. (2015). Potential of the TROPOspheric Monitoring Instrument (TROPOMI) onboard the Sentinel-5 Precursor for the monitoring of terrestrial chlorophyll fluorescence. *Atmospheric Measurement Techniques*, *8*, 1337–1352. https://doi.org/10.5194/amt-8-1337-2015

Guanter, L., Zhang, Y., Jung, M., Joiner, J., Voigt, M., Berry, J. A., … Moran, M. S. (2014). Global and time-resolved monitoring of crop photosynthesis with chlorophyll fluorescence. *Proceedings of the National Academy of Sciences*, *111*, E1327–E1333. https://doi.org/10.1073/pnas.1320008111

Hari, P., & Kulmala, M. (2005). Station for measuring ecosystem-atmosphere relations (SMEAR II). *Boreal Environment Research*, *10*, 351–322.

Hari, P., Mäkelä, A., Korpilahti, E., & Holmberg, M. (1986). Optimal control of gas exchange. *Tree Physiology*, *2*, 169–175. https://doi.org/10.1093/treephys/2.1-2-3.169

Horton, P., Ruban, A. V., Rees, D., Pascal, A. A., Noctor, G., & Young, A. J. (1991). Control of the light-harvesting function of chloroplast membranes by aggregation of the LHCII chlorophyll-protein complex. *FEBS Letters*, *292*, 1–4.

Huang, W., Yang, Y. J., Hu, H., & Zhang, S. B. (2016). Seasonal variations in photosystem I compared with photosystem II of three alpine evergreen broad-leaf tree species. *Journal of Photochemistry and Photobiology B: Biology*, *165*, 71–79. https://doi.org/10.1016/j.jphotobiol.2016.10.014

Idle, D. B., & Proctor, C. W. (1983). An integrating sphere leaf chamber. *Plant, Cell and Environment*, *6*, 437–439. https://doi.org/10.1111/j.1365-3040.1983.tb01279.x

IPCC-SR15 (2018). Special report IPCC. *"Global Warming of 1.5°C."*

Jahns, P., & Holzwarth, A. R. (2012). The role of the xanthophyll cycle and of lutein in photoprotection of photosystem II. *Biochimica et Biophysica Acta - Bioenergetics*, *1817*, 182–193. https://doi.org/10.1016/j.bbabio.2011.04.012

Joiner, J., Yoshida, Y., Guanter, L., & Middleton, E. M. (2016). New methods for the retrieval of chlorophyll red fluorescence from hyperspectral satellite instruments: Simulations and application to GOME-2 and SCIAMACHY. *Atmospheric Measurement Techniques*, *9*, 3939–3967. https://doi.org/10.5194/amt-9-3939-2016

Kitajima, M., & Butler, W. L. (1975). Quenching of chlorophyll fluorescence and primary photochemistry in chloroplasts by dibromothymoquinone. *Biochimica et Biophysica Acta*, *376*, 105–115. https://doi.org/10.1016/0005-2728(75)90209-1

Köhler, P., Frankenberg, C., Magney, T. S., Guanter, L., Joiner, J., & Landgraf, J. (2018). Global retrievals of solar-induced chlorophyll fluorescence with TROPOMI: First results and intersensor comparison to OCO-2. *Geophysical Research Letters*, *45*, 10,456–10,463. https://doi.org/10.1029/2018GL079031

Kolari, P., Bäck, J., Taipale, R., Ruuskanen, T. M., Kajos, M. K., Rinne, J., … Hari, P. (2012). Evaluation of accuracy in measurements of VOC emissions with dynamic chamber system. *Atmospheric Environment*, *62*, 344–351. https://doi.org/10.1016/j.atmosenv.2012.08.054

Kolari, P., Chan, T., Porcar-Castell, A., Bäck, J., Nikinmaa, E., & Juurola, E. (2014). Field and controlled environment measurements show strong seasonal acclimation in photosynthesis and respiration potential in boreal Scots pine. *Frontiers in Plant Science*, *5*, 717.

Kolari, P., Lappalainen, H. K., Hänninen, H., & Hari, P. (2007). Relationship between temperature and the seasonal course of photosynthesis in Scots pine at northern timberline and in southern boreal zone. *Tellus B: Chemical and Physical Meteorology*, *59B*, 542–552.

Lee, J.-E., Berry, J. A., van der Tol, C., Yang, X., Guanter, L., Damm, A., … Frankenberg, C. (2015). Simulations of chlorophyll fluorescence incorporated into the Community Land Model version 4. *Global Change Biology*, *21*, 3469–3477. https://doi.org/10.1111/gcb.12948

Li, X., Xiao, J., He, B., Arain, M. A., Beringer, J., Desai, A. R., … Varlagin, A. (2018). Solar-induced chlorophyll fluorescence is strongly correlated with terrestrial photosynthesis for a wide variety of biomes: First global analysis based on OCO-2 and flux tower observations. *Global Change Biology*, *24*, 3990–4008. 1–19. https://doi.org/10.1111/gcb.14297

Liu, W., Atherton, J., Mõttus, M., Gastellu-Etchegorry, J. P., Malenovský, Z., Raumonen, P., … Porcar-Castell, A. (2019). *Simulating solar-induced chlorophyll fluorescence in a boreal forest stand reconstructed from terrestrial laser scanning measurements* (p. 111274). *Remote Sensing of Environment* in press. https://doi.org/10.1016/j.rse.2019.111274

Lu, X., Cheng, X., Li, X., & Tang, J. (2018). Opportunities and challenges of applications of satellite-derived sun-induced fluorescence at relatively high spatial resolution. *Science of the Total Environment*, *619–620*, 649–653. https://doi.org/10.1016/j.scitotenv.2017.11.158

Macbean, N., Maignan, F., Bacour, C., Lewis, P., Guanter, L., Köhler, P., … Disney, M. (2018). Strong constraint on modelled global carbon uptake using solar-induced chlorophyll fluorescence data. *Scientific reports*, *8*, 1973. 1–12. https://doi.org/10.1038/s41598-018-20024-w

Magney, T. S., Bowling, D. R., Logan, B., Grossmann, K., Stutz, J., Blanken, P., … Frankenberg, C. (2019). Mechanistic evidence for tracking the seasonality of photosynthesis with solar-induced fluorescence. *Proceedings of the National Academy of Sciences*, *116*, 11640–11645. https://doi.org/10.1073/pnas.1900278116

Magney, T. S., Frankenberg, C., Khler, P., North, G., Davis, T. S., Dold, C., … Porcar-Castell, A. (2019). Disentangling changes in the spectral shape of chlorophyll fluorescence: Implications for remote sensing of photosynthesis. *Journal of Geophysical Research: Biogeosciences*, *124*, 1–17. https://doi.org/10.1029/2019JG005029

Majasalmi, T., Stenberg, P., & Rautiainen, M. (2017). Comparison of ground and satellite-based methods for estimating stand-level fPAR in a boreal forest. *Agricultural and Forest Meteorology*, 232, 422–432. https://doi.org/10.1016/j.agrformet.2016.09.007

Malnoë, A. (2018). Photoinhibition or photoprotection of photosynthesis? Update on the (newly termed) sustained quenching component qH. *Environmental and Experimental Botany*, 154, 123–133. https://doi.org/10.1016/j.envexpbot.2018.05.005

Meroni, M., Rossini, M., Guanter, L., Alonso, L., Rascher, U., Colombo, R., & Moreno, J. (2009). Remote sensing of solar-induced chlorophyll fluorescence: Review of methods and applications. *Remote Sensing of Environment*, 113, 2037–2051. https://doi.org/10.1016/j.rse.2009.05.003

Migliavacca, M., Perez-Priego, O., Rossini, M., El-Madany, T. S., Moreno, G., van der Tol, C., ... Reichstein, M. (2017). Plant functional traits and canopy structure control the relationship between photosynthetic CO_2 uptake and far-red sun-induced fluorescence in a Mediterranean grassland under different nutrient availability. *New Phytologist*, 214, 1078–1091. https://doi.org/10.1111/nph.14437

Miloslavina, Y., Wehner, A., Lambrev, P. H., Wientjes, E., Reus, M., Garab, G., ... Holzwarth, A. R. (2008). Far-red fluorescence: A direct spectroscopic marker for LHCII oligomer formation in non-photochemical quenching. *FEBS Letters*, 582, 3625–3631. https://doi.org/10.1016/j.febslet.2008.09.044

Monteith, J. L. (1972). Solar radiation and productivity in tropical ecosystems. *Journal of Applied Ecology*, 9, 747–766. https://doi.org/10.2307/2401901

Murata, N., Takahashi, S., Nishiyama, Y., & Allakhverdiev, S. I. (2007). Photoinhibition of photosystem II under environmental stress. *Biochimica et Biophysica Acta - Bioenergetics*, 1767, 414–421. https://doi.org/10.1016/j.bbabio.2006.11.019

Murchie, E. H., & Lawson, T. (2013). Chlorophyll fluorescence analysis: A guide to good practice and understanding some new applications. *Journal of Experimental Botany*, 64, 3983–3998. https://doi.org/10.1093/jxb/ert208

Nichol, C., Drolet, G., Porcar-Castell, A., Wade, T., Sabater, N., Middleton, E., ... Atherton, J. (2019). Seasonal solar induced chlorophyll fluorescence and photosynthesis in a boreal Scots pine canopy. *Remote Sensing*, 11, 273. https://doi.org/10.3390/rs11030273

Olascoaga, B., Mac, A. A., Atherton, J., & Porcar-Castell, A. (2016). A comparison of methods to estimate photosynthetic light absorption in leaves with contrasting morphology. *Tree Physiology*, 36, 368–379. https://doi.org/10.1093/treephys/tpv133

Öquist, G., Chow, W. S., & Anderson, J. M. (1992). Photoinhibition of photosynthesis represents a mechanism for the long-term regulation of photosystem II. *Planta*, 186, 450–460. https://doi.org/10.1007/BF00195327

Öquist, G., Hällgren, J. E., & Brunes, L. (1978). An apparatus for measuring photosynthetic quantum yields and quanta absorption spectra of intact plants. *Plant, Cell and Environment*, 1, 21–27. https://doi.org/10.1111/j.1365-3040.1978.tb00741.x

Öquist, G., & Huner, N. P. A. (2003). Photosynthesis of overwintering evergreen plants. *Annual Review of Plant Biology*, 54, 329–355. https://doi.org/10.1146/annurev.arplant.54.072402.115741

Ottander, C., Campbell, D., & Öquist, G. (1995). Seasonal changes in photosystem II organisation and pigment composition in *Pinus sylvestris*. *Planta*, 197, 176–183. https://doi.org/10.1007/BF00239954

Ottander, C., & Öquist, G. (1991). Recovery of photosynthesis in winter-stressed Scots pine. *Plant, Cell and Environment*, 14, 345–349. https://doi.org/10.1111/j.1365-3040.1991.tb01511.x

Palombi, L., Cecchi, G., Lognoli, D., Raimondi, V., Toci, G., & Agati, G. (2011). A retrieval algorithm to evaluate the photosystem I and photosystem II spectral contributions to leaf chlorophyll fluorescence at physiological temperatures. *Photosynthesis Research*, 108, 225–239. https://doi.org/10.1007/s11120-011-9678-5

Parazoo, N. C., Arneth, A., Pugh, T. A. M., Smith, B., Steiner, N., Luus, K., ... Miller, C. (2018). Spring photosynthetic onset and net CO_2 uptake in Alaska triggered by landscape thawing. *Global Change Biology*, 24, 3416–3435. https://doi.org/10.1111/gcb.14283

Parazoo, N. C., Bowman, K., Fisher, J. B., Frankenberg, C., Jones, D. B. A., Cescatti, A., ... Montagnani, L. (2014). Terrestrial gross primary production inferred from satellite fluorescence and vegetation models. *Global Change Biology*, 20, 3103–3121. https://doi.org/10.1111/gcb.12652

Pfündel, E. (1998). Estimating the contribution of photosystem I to leaf chlorophyll fluorescence. *Photosynthesis Research*, 56, 185–195. https://doi.org/10.1023/A:1006032804606

Pfündel, E. E., Klughammer, C., Meister, A., & Cerovic, Z. G. (2013). Deriving fluorometer-specific values of relative PSI fluorescence intensity from quenching of F_0 fluorescence in leaves of *Arabidopsis thaliana* and *Zea mays*. *Photosynthesis Research*, 114, 189–206. https://doi.org/10.1007/s11120-012-9788-8

Pirinen P., Simola H., Aalto J., Kaukoranta J.-P., Karlsson P. & Ruuhela R. (2012) Tilastoja suomen ilmastosta 1981-2010. (Climatological statistics of Finland 1981–2010).

Porcar-Castell, A. (2011). A high-resolution portrait of the annual dynamics of photochemical and non-photochemical quenching in needles of *Pinus sylvestris*. *Physiologia Plantarum*, 143, 139–153. https://doi.org/10.1111/j.1399-3054.2011.01488.x

Porcar-Castell, A., Garcia-Plazaola, J. I., Nichol, C. J., Kolari, P., Olascoaga, B., Kuusinen, N., ... Nikinmaa, E. (2012). Physiology of the seasonal relationship between the photochemical reflectance index and photosynthetic light use efficiency. *Oecologia*, 170, 313–323. https://doi.org/10.1007/s00442-012-2317-9

Porcar-Castell, A., Juurola, E., Ensminger, I., Berninger, F., Hari, P., & Nikinmaa, E. (2008). Seasonal acclimation of photosystem II in *Pinus sylvestris*. II. Using the rate constants of sustained thermal energy dissipation and photochemistry to study the effect of the light environment. *Tree physiology*, 28, 1483–1491.

Porcar-Castell, A., Mac, A. A., Rossini, M., Eklundh, L., Pacheco-Labrador, J., Anderson, K., ... Vescovo, L. (2015). EUROSPEC: At the interface between remote-sensing and ecosystem CO_2 flux measurements in Europe. *Biogeosciences*, 12, 6103–6124. https://doi.org/10.5194/bg-12-6103-2015

Porcar-Castell, A., Pfündel, E., Korhonen, J. F. J., & Juurola, E. (2008). A new monitoring PAM fluorometer (MONI-PAM) to study the short- and long-term acclimation of photosystem II in field conditions. *Photosynthesis Research*, 96, 173–179. https://doi.org/10.1007/s11120-008-9292-3

Porcar-Castell, A., Tyystjärvi, E., Atherton, J., van der Tol, C., Flexas, J., Pfündel, E. E., ... Berry, J. A. (2014). Linking chlorophyll a fluorescence to photosynthesis for remote sensing applications: Mechanisms and challenges. *Journal of Experimental Botany*, 65, 4065–4095. https://doi.org/10.1093/jxb/eru191

Quéré, C. L., Andrew, R. M., Friedlingstein, P., Sitch, S., Hauck, J., Pongratz, J., ... Zheng, B. (2018). Global carbon budget 2018. *Earth System Science Data*, 10, 2141–2194.

Raczka B., Porcar-Castell A., Magney T., Lee J.E., Köhler P., Frankenberg C., ... Bowling D.R. (2019) Sustained Non-photochemical Quenching Shapes the Seasonal Pattern of Solar-Induced Fluorescence at a High-Elevation Evergreen Forest. *Journal of Geophysical Research: Biogeosciences* 124.

Rajewicz, P., Atherton, J., Alonso, L., & Porcar-Castell, A. (2019). Leaf-level spectral fluorescence measurements: Comparing methodologies for broadleaves and needles. *Remote Sensing*, 11, 1–20.

Rascher, U., Alonso, L., Burkart, A., Cilia, C., Cogliati, S., Colombo, R., … Zemek, F. (2015). Sun-induced fluorescence—A new probe of photosynthesis: First maps from the imaging spectrometer *HyPlant*. *Global Change Biology*, 21, 4673–4684. https://doi.org/10.1111/gcb.13017

Romero, J. M., Cordon, G. B., & Lagorio, M. G. (2018). Modeling re-absorption of fluorescence from the leaf to the canopy level. *Remote Sensing of Environment*, 204, 138–146. https://doi.org/10.1016/j.rse.2017.10.035

Ruban, A. V. (2016). Nonphotochemical chlorophyll fluorescence quenching: Mechanism and effectiveness in protecting plants from photodamage. *Plant Physiology*, 170, 1903–1916. https://doi.org/10.1104/pp.15.01935

Ruban, A. V. (2018). Light harvesting control in plants. *FEBS Letters*, 592, 3030–3039. https://doi.org/10.1002/1873-3468.13111

Ruban, A. V., Johnson, M. P., & Duffy, C. D. P. (2012). The photoprotective molecular switch in the photosystem II antenna. *Biochimica et Biophysica Acta*, 1817, 167–181.

Smith P., Bustamante M., Ahammad H., Clark H., Dong H., Elsiddig E.A., … Tubiello F. N. (2014) Agriculture, Forestry and Other Land Use (AFOLU). *Climate Change 2014:* Mitigation of Climate Change. Contribution of Working Group III to the Fifth Assessment Report of the Intergovernmental Panel on Climate Change, 811–922.

Smith, W. K., Biederman, J. A., Scott, R. L., Moore, D. J. P., He, M., Kimball, J. S., … Litvak, M. E. (2018). Chlorophyll fluorescence better captures seasonal and interannual gross primary productivity dynamics across dryland ecosystems of southwestern North America. *Geophysical Research Letters*, 45, 748–757. https://doi.org/10.1002/2017GL075922

Sonoike, K. (2011). Photoinhibition of Photosystem I. *Physiologia Plantarum*, 142, 56–64. https://doi.org/10.1111/j.1399-3054.2010.01437.x

Soukupová, J., Cséfalvay, L., Urban, O., Košvancová, M., Marek, M., Rascher, U., & Nedbal, L. (2008). Annual variation of the steady-state chlorophyll fluorescence emission of evergreen plants in temperate zone. *Functional Plant Biology*, 35, 63–76. https://doi.org/10.1071/FP07158

Springer, K. R., Wang, R., & Gamon, J. A. (2017). Seasonal patterns of photosynthesis, fluorescence, and reflectance indices in boreal trees. *Remote Sensing*, 9, 1–18.

Sun, Y., Frankenberg, C., Jung, M., Joiner, J., Guanter, L., Köhler, P., & Magney, T. (2018). Overview of solar-induced chlorophyll fluorescence (SIF) from the orbiting carbon observatory-2: Retrieval, cross-mission comparison, and global monitoring for GPP. *Remote Sensing of Environment*, 209, 808–823. https://doi.org/10.1016/j.rse.2018.02.016

Sun, Y., Frankenberg, C., Wood, J. D., Schimel, D. S., Jung, M., Guanter, L., … Yuen, K. (2017). OCO-2 advances photosynthesis observation from space via solar-induced chlorophyll fluorescence. *Science*, 358, eaam5747.

Thum, T., Zaehle, S., Köhler, P., Aalto, T., Aurela, M., Guanter, L., … Markkanen, T. (2017). Modelling sun-induced fluorescence and photosynthesis with a land surface model at local and regional scales in northern Europe. *Biogeosciences*, 14, 1969–1987. https://doi.org/10.5194/bg-14-1969-2017

van der Tol, C., Berry, J. A., Campbell, P. K. E., & Rascher, U. (2014). Models of fluorescence and photosynthesis for interpreting measurements of solar-induced chlorophyll fluorescence. *Journal of Geophysical Research: Biogeosciences*, 119, 2312–2327. https://doi.org/10.1002/2014JG002713

Van Wittenberghe, S., Alonso, L., Verrelst, J., Moreno, J., & Samson, R. (2015). Bidirectional sun-induced chlorophyll fluorescence emission is influenced by leaf structure and light scattering properties—A bottom-up approach. *Remote Sensing of Environment*, 158, 169–179. https://doi.org/10.1016/j.rse.2014.11.012

Verhoeven, A. (2014). Sustained energy dissipation in winter evergreens. *New Phytologist*, 201, 57–65. https://doi.org/10.1111/nph.12466

Verrelst, J., Rivera, J. P., van der Tol, C., Magnani, F., Mohammed, G., & Moreno, J. (2015). Global sensitivity analysis of the SCOPE model: What drives simulated canopy-leaving sun-induced fluorescence? *Remote Sensing of Environment*, 166, 8–21. https://doi.org/10.1016/j.rse.2015.06.002

Verrelst, J., van der Tol, C., Magnani, F., Sabater, N., Rivera, J. P., Mohammed, G., & Moreno, J. (2016). Evaluating the predictive power of sun-induced chlorophyll fluorescence to estimate net photosynthesis of vegetation canopies: A SCOPE modeling study. *Remote Sensing of Environment*, 176, 139–151. https://doi.org/10.1016/j.rse.2016.01.018

Walther, S., Voigt, M., Thum, T., Gonsamo, A., Zhang, Y., Kohler, P., … Guanter, L. (2016). Satellite chlorophyll fluorescence measurements reveal large-scale decoupling of photosynthesis and greenness dynamics in boreal evergreen forests. *Global Change Biology*, 22, 2979–2996. https://doi.org/10.1111/gcb.13200

Wellburn, A. R. (1994). Spectral determination of chlorophylls *a* and *b*, as well as total carotenoids, using various solvents with spectrophotometers of different resolution. *Journal of Plant Physiology*, 144, 307–313. https://doi.org/10.1016/S0176-1617(11)81192-2

Wieneke, S., Burkart, A., Cendrero-Mateo, M. P., Julitta, T., Rossini, M., Schickling, A., … Rascher, U. (2018). Linking photosynthesis and sun-induced fluorescence at sub-daily to seasonal scales. *Remote Sensing of Environment*, 219, 247–258. https://doi.org/10.1016/j.rse.2018.10.019

Wong, C. Y. S., & Gamon, J. A. (2015). The photochemical reflectance index provides an optical indicator of spring photosynthetic activation in evergreen conifers. *New Phytologist*, 206, 196–208. https://doi.org/10.1111/nph.13251

Yang, P., & van der Tol, C. (2018). Linking canopy scattering of far-red sun-induced chlorophyll fluorescence with reflectance. *Remote Sensing of Environment*, 209, 456–467. https://doi.org/10.1016/j.rse.2018.02.029

Yang P., van der Tol C., Verhoef W., Damm A., Schickling A., Kraska T., Muller O. Rascher U. (2018) Using reflectance to explain vegetation biochemical and structural effects on sun-induced chlorophyll fluorescence. Remote Sensing of Environment., 110996. https://doi.org/10.1016/j.rse.2018.11.039

Zarco-Tejada, P. J., Catalina, A., González, M. R., & Martín, P. (2013). Relationships between net photosynthesis and steady-state chlorophyll fluorescence retrieved from airborne hyperspectral imagery. *Remote Sensing of Environment*, 136, 247–258. https://doi.org/10.1016/j.rse.2013.05.011

Zarco-Tejada, P. J., González-Dugo, M. V., & Fereres, E. (2016). Seasonal stability of chlorophyll fluorescence quantified from airborne hyperspectral imagery as an indicator of net photosynthesis in the context of precision agriculture. *Remote Sensing of Environment*, 179, 89–103. https://doi.org/10.1016/j.rse.2016.03.024

Zarter, C. R., Adams, W. W., Ebbert, V., Cuthbertson, D. J., Adamska, I., & Demmig-Adams, B. (2006). Winter down-regulation of intrinsic photosynthetic capacity coupled with up-regulation of Elip-like proteins and persistent energy dissipation in a subalpine forest. *New Phytologist*, 172, 272–282. https://doi.org/10.1111/j.1469-8137.2006.01815.x

Zarter, C. R., Demmig-Adams, B., Ebbert, V., Adamska, I., & Adams, W. W. (2006). Photosynthetic capacity and light harvesting efficiency during

the winter-to-spring transition in subalpine conifers. *New Phytologist, 172*, 283–292. https://doi.org/10.1111/j.1469-8137.2006.01816.x

Zhang, Y., Guanter, L., Joiner, J., Song, L., & Guan, K. (2018). Spatially-explicit monitoring of crop photosynthetic capacity through the use of space-based chlorophyll fluorescence data. *Remote Sensing of Environment, 210*, 362–374. https://doi.org/10.1016/j.rse.2018.03.031

Zuromski, L. M., Bowling, D. R., Köhler, P., Frankenberg, C., Goulden, M. L., Blanken, P. D., & Lin, J. C. (2018). Solar-induced fluorescence detects interannual variation in gross primary production of coniferous forests in the western United States. *Geophysical Research Letters, 45*, 7184–7193. https://doi.org/10.1029/2018GL077906

SUPPORTING INFORMATION

Additional supporting information may be found online in the Supporting Information section at the end of the article.

Figure S1. Seasonal changes in CO_2 flux, α, β, α_n, and β_n, for each individual chamber.

Figure S2. Seasonal variation of leaf total PAR absorption ($A_{T(PAR)}$).

Figure S3. Linear regression correlations of field F_V/F_M (FMS-2) with field F_V/F_M (MONI-PAM) and lab F_V/F_M (FMS-2).

Figure S4. The significance matrix of Pearson correlation (P) between key study variables.

Figure S5. Coefficients of determination of the linear regression of individual spectral ChlF with Φ_F and integral spectral ChlF ($\int_{660}^{780} F\, d\lambda$).